Aerodynamic Effects of Inferior Turbinate Reduction

Computational Fluid Dynamics Simulation

David Wexler, MD; Rebecca Segal, PhD; Julia Kimbell, PhD

Objective: To investigate the aerodynamic consequences of conservative unilateral inferior turbinate reduction using computational fluid dynamics methods to accomplish detailed nasal airflow simulations.

Design: A high-resolution, finite-element mesh of the nasal airway was constructed from magnetic resonance imaging data of a healthy man. Steady-state, inspiratory airflow simulations were conducted at 15 L/min using the techniques of computational fluid dynamics

Intervention: Circumferential removal of 2 mm of soft tissue bulk along the length of the left inferior turbinate was modeled.

Main Outcome Measures: Nasal airflow distribution and pressure profiles were computed before and after simulated left inferior turbinate reduction.

Results: Simulated inferior turbinate reduction resulted in a broad reduction of pressure along the nasal airway, including the regions distant from the inferior turbinate vicinity. In contrast, relative airflow changes were regional: airflow was minimally affected in the valve region, increased in the lower portion of the middle and posterior nose, and decreased dorsally.

Conclusion: Use of computational fluid dynamics methods should help elucidate the aerodynamic significance of specific surgical interventions and refine surgical approaches to the nasal airway.

Arch Otolaryngol Head Neck Surg. 2005;131:1102-1107

INFERIOR TURBINATE REDUCTION (ITR) surgery is often performed for chronic nasal obstruction attributed to refractory turbinate enlargement. Numerous techniques for ITR have been reported,[1,2] and most studies indicate a significant rate of clinical success in improving nasal patency. The amount of tissue reduction needed to achieve positive results is uncertain. Some investigators[3-6] have reported that partial turbinectomy methods are effective, whereas others[7,8] have advocated total turbinectomy. Partial turbinectomy itself can take a variety of forms, and various surgical techniques may be used. In most ITR studies, the available outcome data consist of subjective measures of satisfaction with the nasal airway. Although these studies provide important information, the physiologic interpretation of such subjective measures is limited. Therefore, it is desirable to quantify the effects of ITR on nasal airflow and pressure-flow relationships.

The standard quantitative approach to physiologic assessment of the nasal airway is rhinomanometry.[9] Air pressure (P) and flow (Q) can readily be measured using rhinomanometry, enabling the determination of nasal resistance (R) using the formula $\Delta P = Q \times R$. A reduction of 62.5% to 75% in total nasal resistance has been shown 1 year after ITR procedures.[1] With total turbinectomy,[10] a 56.8% reduction in nasal resistance was documented at 1 year. There are, however, certain limitations with the rhinomanometric approach. The state of nasal vasocongestion at any given time will greatly affect the resistance determination and could obscure and confound interpretation of the direct surgical effect. Even with topical decongestion to reduce this congestion factor, there is a lack of correlative geometric information regarding the location and amount of tissue reduction that produces specific local and transnasal aerodynamic effects.

Using a theoretical approach, one could construct a model of the nasal passages and apply the methods of fluid mechanics to compute the detailed airflow and pressure information. Then pressure and airflow data could be recomputed after a specific simulated surgical intervention on the model to demonstrate the aerodynamic consequences of the surgery. The governing equations for fluid flow through a conduit are precisely described by the Navier-Stokes equations.[11] Since formulation of the Navier-Stokes equations nearly 200 years ago, exact mathematical solutions have been found only for the simplest geometric configurations. It is only with the advent of computational fluid dynamics

Author Affiliations: Division of Otolaryngology, Fallon Clinic, Worcester, Mass (Dr Wexler); and CIIT Centers for Health Research, Research Triangle Park, NC (Drs Segal and Kimbell).

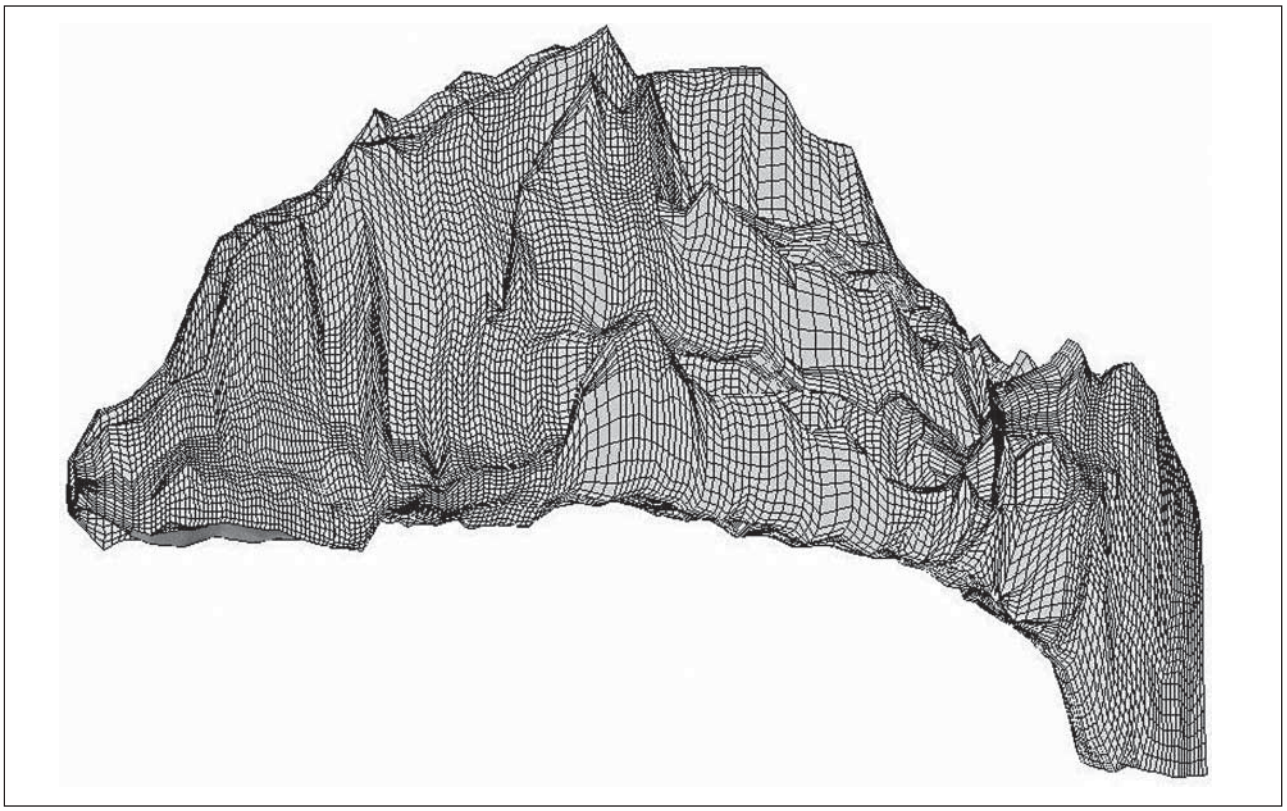

Figure 1. Lateral view of the finite element grid used in this study.[12] The nostrils are on the left and the nasopharynx is on the right.

(CFD) methods and powerful computer technology that solutions to the Navier-Stokes equations can be closely approximated by numerical methods and applied to complex conduit shapes such as that of the nose.

Detailed nasal airflow analysis has been undertaken in various human nasal models.[12-15] At lower airspeeds, which correspond to resting breathing rates, airflow is predominantly laminar, and the models yield pressure and velocity data similar to those obtained in large-scale laboratory physical models.[12,14,16] Descriptions of the potential utility of CFD for the analysis of nasal surgical planning have been reported,[13,17-19] but data on the effects of ITR are limited. A recent study[17] using CFD found increased turbulent effects after total turbinectomy but did not present the detailed pressure and flow analysis.

In the present study, we modified an established CFD model of a human nose[12] to determine the aerodynamic effects of a unilateral ITR procedure. This effort constitutes our first step toward the goal of developing an approach to the mathematical analysis of nasal airway surgery. In addition, the findings should provide insights into nasal aerodynamics of general physiologic interest.

METHODS

This study was based on a human nasal model previously reported in detail.[12] The highlights are summarized herein to familiarize the reader with the methods. The patient on whom the mathematical model was based was a healthy, nonsmoking, 53-year-old white man with no nasal complaints or history of sinonasal disease. A magnetic resonance image of the head was obtained consisting of a coronal reconstruction in serial 3-mm sections. A 3-dimensional, high-resolution finite element mesh was generated from digitized tracings of the magnetic resonance imaging coronal sections, with intermediate sections estimated using computer-aided design software[20] between adjacent magnetic resonance images. The resulting finite element grid had 165 083 interconnected nodes forming 135 360 six-sided brick-shaped elements (**Figure 1**). For this investigation, a quiescent cyclic breathing rate of 7.5 L/min (125 mL/s) was chosen. Because the computational model simulated steady-state (noncyclic) airflow, the total nasal inspiratory airflow rate was set to 15 L/min. This fixed airflow rate was imposed at the nostrils, with a uniform velocity profile (plug flow) apportioned between the left and right nostrils according to the cross-sectional area (CSA). The right nostril had a CSA of 0.57 cm^2, and the left nostril had a CSA of 0.70 cm^2; accordingly, the assigned airflow was 6.74 L/min on the right (44.9% of the total) and 8.26 L/min on the left (55.1% of the total).

Under steady-state conditions, the Navier-Stokes and continuity equations describing viscous fluid flow[21] are formulated as follows:

$$\rho(u \cdot \nabla u) = -\nabla p + \mu\nabla^2 u$$
$$\nabla \cdot u = 0$$

where ρ is the mass density of air (1.196×10^{-3} g/cm^3); u, the velocity vector having x, y, and z components (in centimeters per second); ∇, the gradient operator, ie;

$$\left(\frac{\partial}{\partial x}, \frac{\partial}{\partial y}, \frac{\partial}{\partial z}\right);$$

p, the pressure (in dynes per square centimeter); μ, the viscosity of air (1.8×10^{-4} g/[cm-sec]); and ∇^2, the Laplacian operator, ie;

$$\left(\frac{\partial^2}{\partial x^2} + \frac{\partial^2}{\partial y^2} + \frac{\partial^2}{\partial z^2}\right).$$

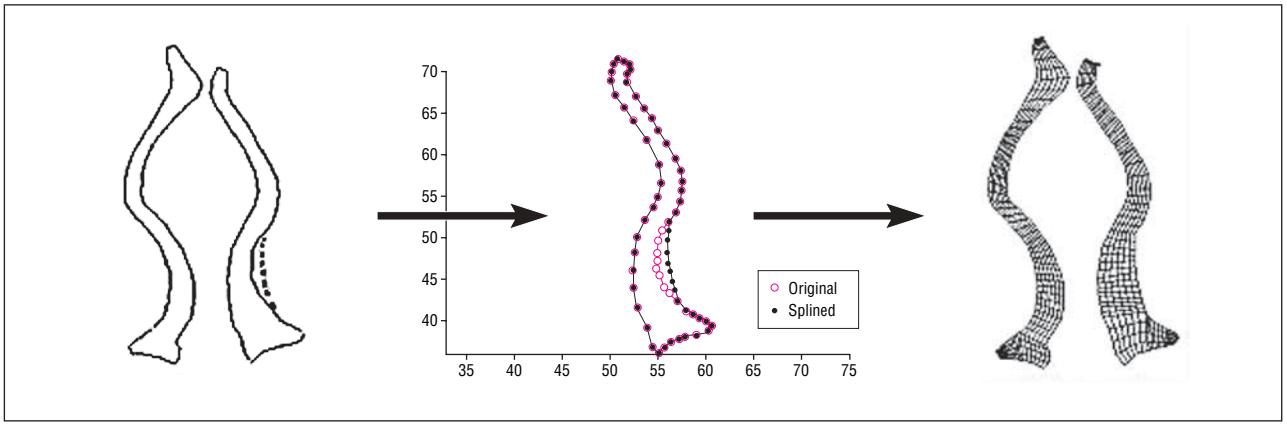

Figure 2. Alteration of the original computational fluid dynamics model to simulate left inferior turbinate reduction (ITR). Left, Original cross section near the anterior end of inferior turbinates, with markings to indicate the extent of the left ITR at that level. Middle, View of the same cross section showing alteration of the boundary points from the original locations to those reflecting left ITR. Right, Cross section of the finite element grid after simulated left ITR at the same cross-sectional level.

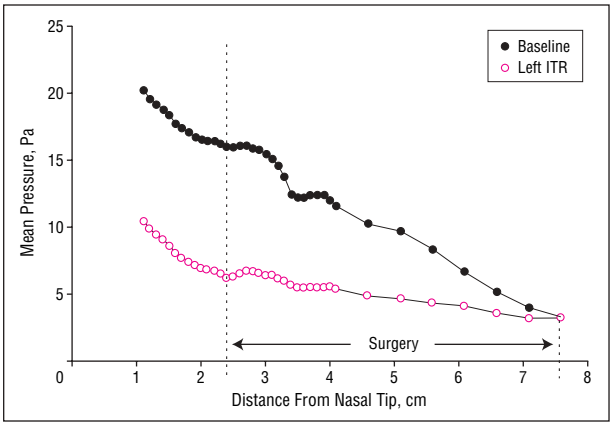

Figure 3. Simulated pressure averaged over only the left side of the coronal cross sections at various levels from just posterior to the nostrils to the nasopharynx. Baseline indicates predictions from the original computational fluid dynamics (CFD) model; left ITR (inferior turbinate reduction), predictions from the modified CFD model.

A software package (FIDAP CFD; Fluent Inc, Lebanon, NH) was used to solve the Navier-Stokes equations for pressure and velocity components at each nodal point in the finite element grid. The main assumptions of the CFD method used herein are steady-state flow and incompressibility of air; the latter is an acceptable assumption at physiologic airflow rates. The boundary conditions were set as follows:

1. A no-slip condition was imposed at airway walls, meaning that air velocity was set to zero at the surface of the nasal membranes.
2. A stress-free condition was imposed at the outlet, meaning that pressure (p) was required to be close to zero at the lower nasopharynx.
3. Plug flow was imposed at the inlet, meaning that all velocity vectors were the same length and of perpendicular orientation to the nostril surfaces.

The results of this airflow simulation are in good agreement with experimental measurements reported in the literature for similar flow rates and were presented and discussed previously.[12]

A left ITR was modeled by modifying the original serial coronal tracings to effect a 2-mm circumferential soft tissue reduction in each section over the full length of the inferior turbinate, with tapering of the tissue reduction at the anterior and posterior ends of the turbinate (**Figure 2**). After construction of the modified finite element mesh, the baseline and modified nasal models were processed using FIDAP CFD. Computational output was visualized using a software program (Fieldview; Intelligent Light, Lyndhurst, NJ). Pressure and airflow data were compared at selected coronal levels before and after the simulated left ITR. Airflow distribution in the nose was determined by calculating volumetric flow allocation across representative coronal sections from anterior, middle nasal, and posterior portions of the model.

RESULTS

Computer-simulated ITR produced a marked broad reduction in intranasal pressures along the full length of the affected nasal passage (**Figure 3**). This reduction in simulated pressure was greatest anteriorly in the nose (approximately 59%) and was less striking in the posterior portion of the nasal passage (approximately 17%) (**Table 1**). Simulated pressure changes were not limited to the immediate vicinity of the inferior turbinate; even the proximal valve region, which had no change in CSA because of the ITR, still had a large reduction in pressure. We found that, in general, the pressure reduction from simulated ITR in a given nasal region did not correlate with enlargement in the CSA in that same region (Table 1). Pressure outputs for representative coronal sections (**Figure 4**) showed that the pressure reduction was manifest diffusely on the side of the ITR (**Figure 5**).

Mean airspeeds from the model showed a trend opposite that of the pressures: mean airspeeds changed little anteriorly, despite the large decline in pressure, whereas mean airspeeds were estimated to decrease more than 20% posteriorly (Table 1). Mean airspeed in the anterior valve region was estimated to be 152 cm/s before ITR and 150.5 cm/s after ITR. Peak airspeeds were approximately double the mean airspeeds in both cases. In fully developed laminar fluid flow, the velocity profile across a cylindrical conduit assumes a parabolic configuration, with the peak velocity being exactly double the mean velocity. Although not a main focus in this study, a sampling of velocity profile plots from the septum to the turbinates in the middle caval region generally showed irregular parabolic forms consistent with disturbed and incompletely developed laminar airflow.

Table 1. Effects of Left Inferior Turbinate Reduction on Left Cross-sectional Area, Mean Pressure, and Mean Airspeed*

	Cross-sectional Area, cm^2†			Pressure,† Mean, Pa			Airspeed, Mean, cm/s†		
	Before	After	Change, %	Before	After	Change, %	Before	After	Change, %
Proximal valve (z = 2.1 cm)	1.19	1.19	0	16.47	6.75	–59.0	152.5	150.5	–1.3
Distal valve (z = 3.1 cm)	0.87	1.02	17.2	15.12	6.39	–57.7	184.8	150.4	–18.6
Anterior cavum (z = 4.1 cm)	1.21	1.50	24.0	11.62	5.42	–53.4	134.0	104.1	–22.3
Middle cavum (z = 5.6 cm)	1.32	1.73	31.1	8.30	4.34	–47.7	124.3	97.1	–21.9
Distal cavum (z = 7.1 cm)	1.56	1.92	23.1	3.99	3.29	–17.5	104.9	79.0	–24.7

*z Refers to the distance from the tip of the nose.
†All data are from the left nasal passage.

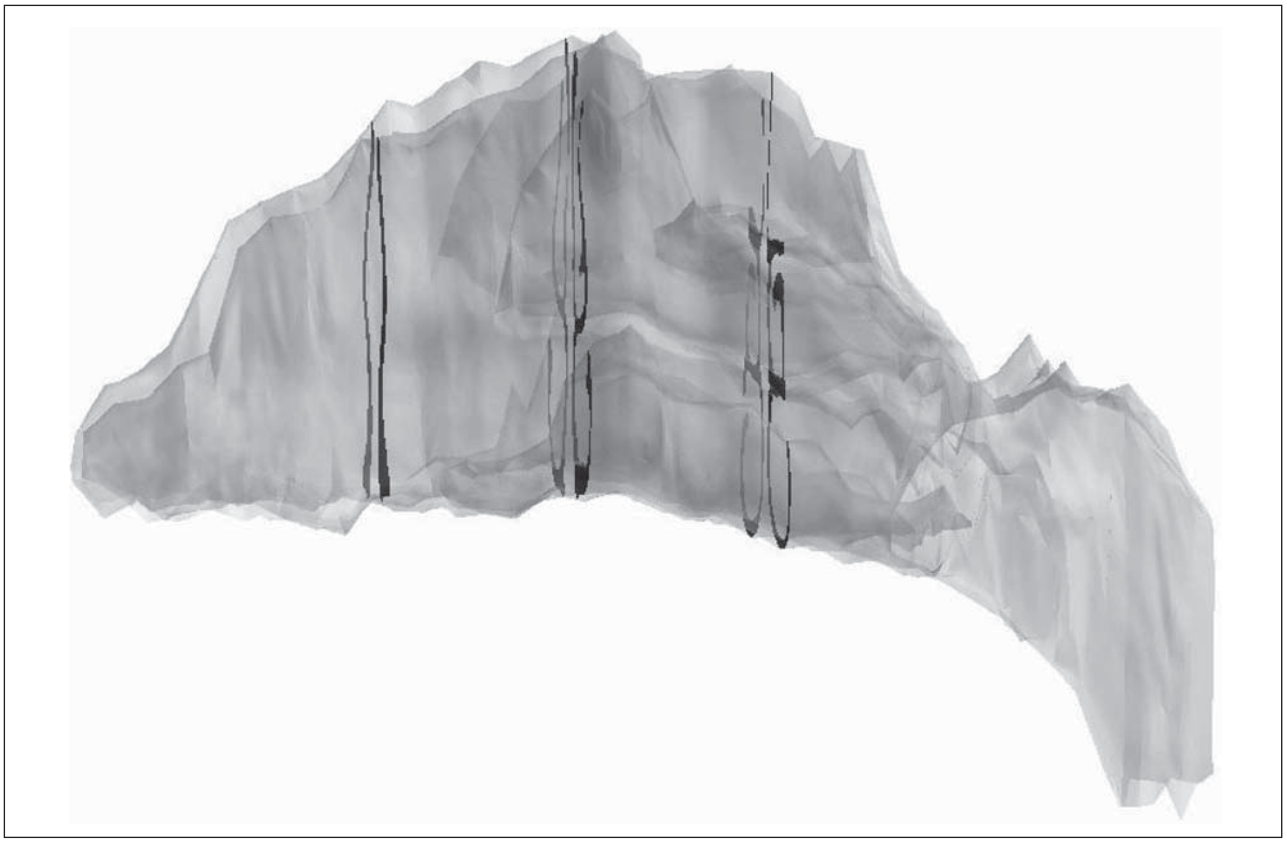

Figure 4. Locations of representative coronal cross sections in the computational fluid dynamics model. The nostrils are on the left and the nasopharynx is on the right.

Simulated ITR also affected relative airflow distribution in the nasal passages (Figure 5 and **Table 2**). After ITR, more air was predicted to flow inferiorly in the passages, with accordingly less airflow in the middle and upper levels of the nasal passages. In the nasal valve region, there was minimal change in relative airflow in the lower and middle levels, whereas the redistribution toward increased inferior nasal airflow was prominent at the middle cavum and posterior cavum levels. Dorsal nasal airflow was reduced from its modest baseline levels at the valve and in the nasal cavum.

COMMENT

The CFD simulations predicted that conservative ITR produces marked changes in nasal pressure, airspeed, and relative airflow distribution throughout the nasal passages. These effects were not localized to the ITR region. For example, a nearly 60% decline in pressure was calculated at the proximal valve region, although virtual tissue reduction in the modeled ITR reached only the distal or bony valve segment.[22] The decrease in simulated pressure at any given coronal level did not correlate with the amount of increase in CSA for that section. These complex responses highlight the sometimes nonintuitive nature of nasal passage aerodynamics and strengthen the case for applying computational methods to the study of nasal surgery.

We recognize that our model, which was based on fixed flow at the nasal inlet, does not reproduce the physiologic situation of a net transnasal pressure difference, which is the usual driving force for airflow. Under true physiologic

conditions, ITR is likely to produce increased airflow for the same transnasal pressure difference rather than a lower pressure decline for fixed airflow, as demonstrated in the present study. Therefore, it is instructive to derive an overall nasal resistance value from our flow and pressure simulations, enabling us to estimate how much airflow should change in the physiologic condition for a given transnasal driving pressure. Using the $\Delta P = Q \times R$ formula for the specified flow rates, the simulated transnasal resistance for the left nasal passage before ITR was 0.125 Pa/cm^3 per second and after ITR was 0.053 Pa/cm^3 per second. Thus, a 57% decline in unilateral nasal resistance resulted from the simulated left ITR. Although our model was based on the nasal anatomy of an asymptomatic individual, the resistance-lowering effect of simulated ITR on nasal resistance was similar to that reported for clinical ITR reduction in patients with nasal obstruction.[1]

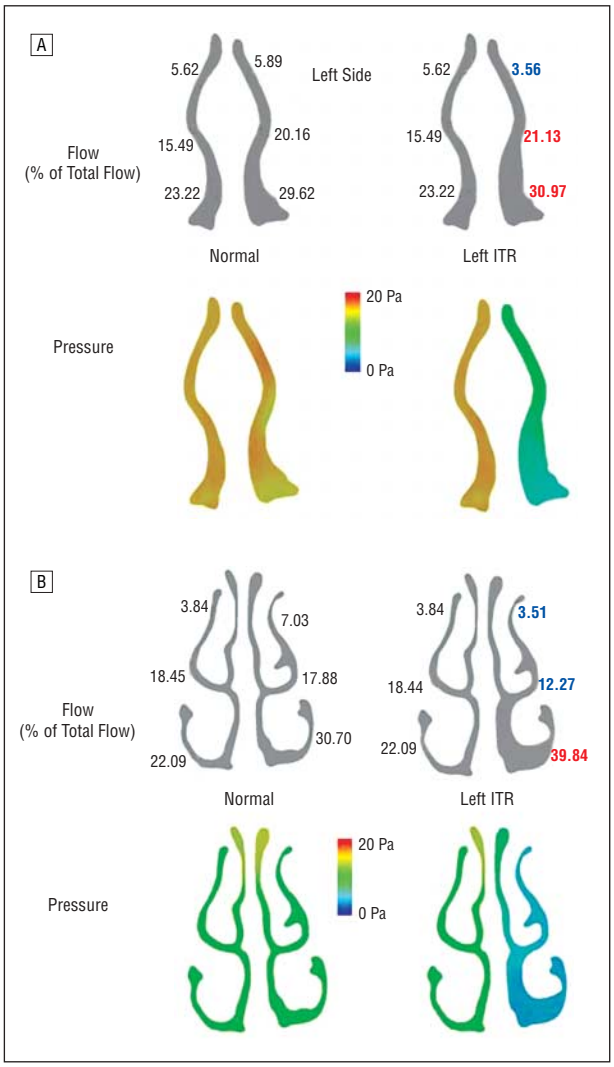

Figure 5. Coronal cross sections showing plots of regional airflow allocation and pressure 2.85 cm (A) and 4.73 cm (B) from the tip of the nose. Colored values and arrows on the upper panels depicting left inferior turbinate reduction (ITR) indicate change from normal (red, increased; blue, decreased).

On the right side (not subjected to turbinate reduction), the simulated resistance was 0.145 Pa/cm^3 per second. Total nasal resistance, calculated using the formula for parallel resistors ($1/R_{total} = 1/R_{left} + 1/R_{right}$) was calculated to be 0.067 Pa/cm^3 per second before left ITR and 0.039 Pa/cm^3 per second after ITR, for an overall reduction in nasal resistance of 42.1%. This dramatic effect, predicted to result from a modest change in inferior turbinate size, suggests that physiologic changes in turbinate size due to variations in the state of vasocongestion would similarly affect nasal airway resistance. For example, topical nasal decongestion was reported to lower nasal resistance by 37%.[9]

The calculated resistance values in the previous paragraph are somewhat lower than reported clinical values,[23] which consisted of mean combined nasal resistances of 0.14 Pa/cm^3 per second in unobstructed noses and 0.09 Pa/cm^3 per second in decongested noses. As Cole[23] noted, nasal airflow resistances are calculated at a given transnasal pressure difference, usually 100 or 150 Pa. Resting tidal breathing in adults generates pressure differences less than 100 Pa, and thus lower resistance values less than 0.10 Pa/cm^3 per second may be found in normal noses.[23]

The transnasal pressure difference between the nostrils and the nasopharynx in the baseline model was predicted to be just greater than 18 Pa at a total bilateral flow rate of 15 L/min. Other investigators,[16,24] using large-scale physical models of the human nose, have also reported relatively low transnasal pressure differences at similar flow rates. This is lower than pressure declines typically recorded in clinical airflow measurements. The difference in pressure declines between CFD/experimental and clinical situations requires further investigation. One concern is the possibility of overestimation of airspace regions because the air–soft tissue interfaces are subjectively selected from the original images. Also, an airflow-induced shift of compliant nasal soft tissues during respiration could narrow the passage and produce a greater transnasal pressure decline than that seen in our fixed-wall model.

Undetected turbulence is another factor that could significantly affect the transnasal resistance estimate in our

Table 2. Relative Airflow Distribution in the Left Nasal Passage Before and After Inferior Turbinate Reduction*

	Lower Third		Middle Third		Upper Third	
	Before	After	Before	After	Before	After
Valve (z = 2.85 cm)	53.1	55.6	36.2	37.9	10.6	6.4
Middle cavum (z = 4.73 cm)	55.1	71.5	32.1	22.1	12.6	6.3
Posterior cavum (z = 6.6 cm)	42.4	61.8	52.2	35.7	5.4	2.5

*Data are given as a percentage of total left nasal airflow for each region of the given coronal section. See Figure 4 for images of these representative sections.
z Refers to the distance from the tip of the nose.

results. Although low airflow rates (<200 mL/s) are generally associated with disturbed- or near-laminar flow in the nose,[16,24] the presence of turbulence would increase the total nasal resistance. Hahn and colleagues[16] measured a mild turbulence intensity of approximately 1.5% to 2.2% at low airflow rates in a large-scale physical model of the nose. Whereas in purely laminar flow the resistance increases in proportion to velocity, with turbulent flow the resistance increases approximately as the square of velocity.[25] The simulations presented herein are based on a numerical solution of the full set of nonlinear Navier-Stokes equations. Although these equations theoretically describe laminar and turbulent flow and secondary flows like swirls, their numerical solution will not fully characterize turbulence due to computational limitations, particularly those related to grid size. Preliminary tests with a higher mesh density have indicated that at 15 L/min, effects due to mesh density are small, on the order of a few percent. Although probably not a major factor for the low flow rates used in the present study, the general issue of turbulence in nasal airflow and nasal modeling needs further clarification.

The numerical model described herein used fixed plug flow at the nostrils, that is, a fixed airflow rate at the nostrils, rather than pulled flow, based on a negative pressure set at the nasopharynx. Preliminary attempts at pulled-flow simulations to date were made by either imposing a pressure decline across the model or specifying outflow velocities. These simulations to date have been unsuccessful for physiologic flow rates owing to failure of the equations to converge, meaning that a reliable numerical solution could not be achieved. The computational difficulty is not yet known for the applied pressure decline case, but in the applied velocities case, it seems to result from the complex flow patterns in the nasopharynx, which make initiation of the flow simulation there difficult. In contrast, at the anterior nasal inlet, airflow is more well behaved as it quickly channels into the nasal valve area. This, in turn, allows for convergence of the iterative numerical methods to produce a usable output. We believe that the development of pulled-flow models, which more directly represent the physiologic inspiratory mechanism, will be worthwhile for further study of nasal aerodynamics.

In summary, CFD methods can be applied to the aerodynamic study of surgically altered nasal airways. There are many methods of turbinate reduction, and the present study examined only 1 relatively conservative reduction pattern. As methods of mesh generation and airflow simulation are improved, a series of comparative simulations should enable determination of optimal anatomic configurations and serve as a guide for planning nasal airway surgery.

Submitted for Publication: January 27, 2005; final revision received July 14, 2005; accepted July 29, 2005.
Correspondence: David Wexler, MD, Division of Otolaryngology, Fallon Clinic, 20 Worcester Center Blvd, Suite 300, Worcester, MA 01608 (david.wexler@fallon-clinic.com).

Financial Disclosure: None.
Funding/Support: This work was funded by the CIIT Centers for Health Research and the American Chemistry Council, Arlington, Va.
Acknowledgment: We thank Regina Richardson, BS, Darin Kalisak, MA, Grace Kepler, PhD, Mel Andersen, PhD, Fred Miller, PhD, Dave Dorman, DVM, PhD, and Barbara Kuyper, PhD, for their contributions and support.

REFERENCES

1. Passali D, Lauriello M, Anselmi M, Bellussi L. Treatment of hypertrophy of the inferior turbinate: long-term results in 382 patients randomly assigned to therapy. *Ann Otol Rhinol Laryngol*. 1999;108:569-575.
2. Mabry RL. Surgery of the inferior turbinates: how much and when? *Otolaryngol Head Neck Surg*. 1984;92:571-576.
3. Friedman M, Tanyeri H, Lim J, et al. A safe, alternate technique for inferior turbinate reduction. *Laryngoscope*. 1999;109:1834-1837.
4. Fanous N. Anterior turbinectomy. *Arch Otolaryngol Head Neck Surg*. 1986;112:850-852.
5. Rakover Y, Rosen G. A comparison of partial inferior turbinectomy and cryosurgery for hypertrophic inferior turbinates. *J Laryngol Otol*. 1996;110:732-735.
6. Yanez C. New technique for turbinate reduction in chronic hypertrophic rhinitis: intraturbinate stroma removal using the microderider. *Operat Tech Otolaryngol Head Neck Surg*. 1998;9:135-137.
7. Ophir D. Inferior turbinectomy. *Operat Tech Otolaryngol Head Neck Surg*. 1991;2:189-193.
8. Talmon Y, Samet A, Gilbey P. Total inferior turbinectomy: operative results and technique. *Ann Otol Rhinol Laryngol*. 2000;109:1117-1119.
9. Cole P. Nasal patency and its measurement. *Am J Rhinol*. 1987;1:135-139.
10. Wight RG, Jones AS, Beckingham E. Trimming of the inferior turbinates: a prospective long-term study. *Clin Otolaryngol*. 1990;15:347-350.
11. Hughes WF, Brighton JA. Mathematical models of fluid motion. In: *Fluid Dynamics*. New York, NY: McGraw-Hill; 1999:34-84.
12. Subramaniam R, Richardson R, Morgan K, Kimbell J. Computational fluid dynamics simulations of inspiratory airflow in the human nose and nasopharynx. *Inhal Toxicol*. 1998;10:91-120.
13. Elad D, Liebenthal R, Wenig B, Einav S. Analysis of air flow patterns in the human nose. *Med Biol Eng Comput*. 1993;31:585-592.
14. Keyhani K, Scherer P, Mozell M. Numerical simulation of airflow in the human nasal cavity. *J Biomech Eng*. 1995;117:429-441.
15. Kelly J, Prasad A, Wexler A. Detailed flow patterns in the nasal cavity. *J Appl Physiol*. 2000;89:323-337.
16. Hahn I, Scherer PW, Mozell MM. Velocity profiles measured for airflow through a large-scale model of the human nasal cavity. *J Appl Physiol*. 1993;75:2273-2287.
17. Weinhold I, Mlynski G. Numerical simulation of airflow in the human nose. *Eur Arch Otorhinolaryngol*. 2004;261:452-455.
18. Horschler I, Meinke M, Schroder W. Numerical simulation of the flow field in a model of the nasal cavity. *Comput Fluids*. 2003;32:39-45.
19. Bockholt U, Mlynski G, Muller W, Voss G. Rhinosurgical therapy planning via endonasal airflow simulation. *Comput Aided Surg*. 2000;5:175-179.
20. Guilmette A, Gagliano TJ. Construction of a model of human nasal airways using in vivo morphometric data. *Ann Occup Hyg*. 1994;38(suppl 1):69-75.
21. Batchelor GK. *An Introduction to Fluid Dynamics*. Cambridge, England: Cambridge University Press; 1967.
22. Wexler DB, Davidson TM. The nasal valve: a review of the anatomy, imaging and physiology. *Am J Rhinol*. 2004;18:143-150.
23. Cole P. Nasal airflow resistance: a survey of 2500 assessments. *Am J Rhinol*. 1997;11:415-420.
24. Schreck S, Sullivan KJ, Ho CM, Chang HK. Correlations between flow resistance and geometry in a model of the human nose. *J Appl Physiol*. 1993;75:1767-1775.
25. Swift D. Physical principles of airflow and transport phenomena influencing air modification. In: Proctor DF, Andersen I, eds. *The Nose, Upper Airway Physiology and the Atmospheric Environment*. Amsterdam, the Netherlands: Elsevier Biomedical Press; 1982.